

INFLUENCE OF APOPHIS' SPIN AXIS VARIATIONS ON A SPACECRAFT DURING THE 2029 CLOSE APPROACH WITH EARTH

SAFWAN ALJBAAE¹, JEAN SOUCHAY², VALERIO CARRUBA³, DIOGO M. SANCHEZ¹,
ANTONIO F. B. A. PRADO¹

¹*Division of Space Mechanics and Control, INPE,
C.P. 515, 12227-310 São José dos Campos, SP, Brazil
Email: safwan.aljbaae@gmail.com*

²*SYRTE, Observatoire de Paris, PSL Research University, CNRS,
Sorbonne Universités, UPMC Univ. Paris 06,
LNE, 61 avenue de l'Observatoire, 75014 Paris, France*

³*São Paulo State University (UNESP),
School of Natural Sciences and Engineering,
Guaratinguetá, SP, 12516-410, Brazil*

Abstract. Tumbling asteroids belong to a group of objects, whose angular velocity vector is unaligned with any of its principal axes of inertia. This rotation state leads to challenges when modelling a spacecraft's orbit around these bodies. In this work, we refine a previous study on this topic, concerning asteroid (99942) Apophis during its close encounter with the Earth in 2029. We analyze the orbital behaviour of a spacecraft orbiting the asteroid during this event by including the effects of the changes of orientation of the spin axis of the asteroid, depending on two sets of initial conditions. We analyze the global dynamics of the spacecraft around the target using three approaches, MEGNO, PMap, and Time-Series prediction. We limited our work on the equatorial plan choosing critical initial conditions of the span orientation of the target. We confirm that no spacecraft with natural orbits (orbits without control) could survive the high perturbations caused by the close encounter with our planet.

Key words: Celestial Mechanics – Dynamical astronomy – Minor planets – Asteroids: individual (Apophis).

1. INTRODUCTION

The near-Earth asteroid 99942 Apophis is a small 387 meters body with a mass between 4.4 and 6.2×10^{10} kg (Brozović *et al.*, 2018; Pravec *et al.*, 2014; Müller *et al.*, 2014). This asteroid is classified as potentially dangerous in the future and it will experience a close encounter with Earth on 2029 April 13, at about 38 000 km from the

Earth's center*. However, impacts with our planets have been ruled out for the next 100 years†. A mission that places a spacecraft in orbit around (99942) Apophis just before the close encounter with our planet would be very important because, for the first time, it could make close-up observations of an asteroid during a close encounter with our planet, which can change the orientation of the spin axis of the target, as well as its shape. In fact, the encounter of Apophis with our planet excites dynamically the motion of any particle located in a zone around the asteroid, possibly causing its collision or escape from the target, as shown by [Aljbaae *et al.* \(2020\)](#). In this last study, possible changes of orientation of the spin axis of the target were neglected. On the contrary, in this paper, our aim is to provide a more complete dynamical analysis of an orbiting spacecraft including these changes. Notice that Apophis is well known to be in a moderately tumbling rotation state ([Pravec *et al.*, 2014](#)), and that the Earth gravitational potential will affect significantly the spin state of the target ([Scheeres *et al.*, 2005](#); [Souchay *et al.*, 2018](#)). The shape of Apophis ([Pravec *et al.*, 2014](#)) that we used in this work is perfectly oriented along its principal axes of inertia ([Aljbaae *et al.*, 2020](#)), which means that the axis of the figure and the angular momentum axis are coinciding, which agrees with the assumption of the asteroid rotates in a short-axis mode, that was used in [Souchay *et al.* \(2018\)](#) to estimate the changes of the angular momentum axis of Apophis. These changes were calculated starting from the two fundamental parameters representing the motion of the Apophis axis in space. These parameters are ϵ , the obliquity angle between the orbital and equatorial plane of the asteroid, and ψ , the precession angle, which expresses the motion of the ascending node of the equator with respect to the orbital plane (Fig. 1).

In this paper, we aim at characterizing the effects of the changes of the spin axis and rate of (99942) Apophis on the motion of a spacecraft orbiting the asteroid. Our work is divided as follows. In Sec. 2 we use the equations of motion of [Souchay *et al.* \(2018\)](#), to recalculate the extreme amplitudes of the effects of the close approach on the Apophis spin axis, according to the range of adequate initial conditions. Then, a complete dynamical model of a spacecraft in orbit around the target is presented in Sec. 3, where we take into account these last effects. In Sec. 4, we calculate the specific effects of the changes of the spin axis of Apophis on the orbit of the spacecraft, depending on two sets of initial conditions. In Sec. 5, we consider the full set of perturbations to characterize the dynamical evolution of a spacecraft around Apophis. We investigate a new approach based on Time-Series Prediction with Machine Learning to identify non-chaotic regions. We compare the results of this new approach to those we obtain from PMap ([Sanchez *et al.*, 2017](#); [Sanchez and Prado ,](#)

* <https://ssd.jpl.nasa.gov/sbdb.cgi?sstr=APophis;orb=0;cov=0;log=0;cad=1#cad>

† <https://www.jpl.nasa.gov/news/nasa-analysis-earth-is-safe-from-asteroid-apophis-for-100-plus-years>

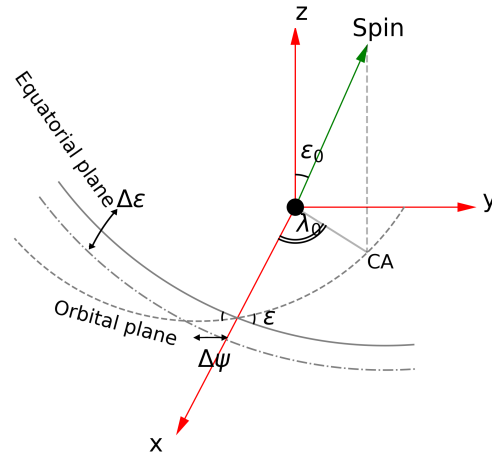


Fig. 1 – Parametrization of the spin axis of Apophis before and after the close encounter. ϵ and ψ are the obliquity and precession angles, respectively.

2019) and MEGNO (Cincotta and Simó, 2000) methods using nearby orbits.

2. VARIATIONS OF THE APOPHIS SPIN AXIS

Pravec *et al.* (2014) used a large set of lightcurves observations to determine the rotational state of Apophis. Their conclusion was that the brightness of Apophis did not repeat with a single period, but it showed the characteristics of a slightly tumbling rotational state. Using a 2-period Fourier series method, they found two components, the main one, with period $P_1 = 30.56\text{h}$, which corresponds to a leading rotation component around the SAM (Short Axis Mode) and a secondary one with a period around $P_2 = 29.05\text{h}$, but with relatively large uncertainty. Pravec *et al.* (2014) mentioned other values fit to the data. The best fit for P2 was obtained with a period of 29.05 h, but there were other periods that gave only slightly poorer fits; the authors mentioned the periods of 32.2 h and 27.5 h. Nevertheless, the amplitude of the wobble around the SAM is rather small, between 20° and 25° , which characterizes a moderate excitation. Whatever the amplitude of the wobble during the 2029 close encounter will be, we considered that during the fly-by the rotational angular rate of the asteroid remains constant. That is certainly not real but the estimation of the amplitude of these variations looks like an open question and out of the scope of this work. We concentrate on the relatively large changes due to Earth's gravity during the close encounter.

Scheeres *et al.* (2005) estimated the changes in the spin-state of Apophis by conducting Monte-Carlo simulations modelling the asteroid as a tri-axial ellipsoid with a length-to-width ratio of 1.4. More recently, Souchay *et al.* (2018) used the classical theory of the rotation of the Earth, originally developed in Kinoshita (1978), to calculate the variations of the orientation of Apophis angular momentum axis during the close encounter due to the tidal deformation associated with the gravitational potential of our planet. The authors used the physical characteristics of the asteroid from Pravec *et al.* (2014). Souchay *et al.* (2018) showed that the values of the spin axis orientation parameters just before the encounter should be bounded in the intervals $[10^\circ - 100^\circ]$ for λ_0 and $[10^\circ - 70^\circ]$ for ε_0 , according to the observational data from Pravec *et al.* (2014). They tested numerous initial values of $(\lambda_0, \varepsilon_0)$ and showed that the asteroid could undergo dramatic changes in obliquity (ε) and longitude of the ascending node (ψ). The formulas leading to the determinations of these changes are given in 6. In this work, we choose to follow the study of Souchay *et al.* (2018) to determine the minimum and maximum values of the amplitudes of changes of the orientation of the spin axis and investigate the effects of these changes on the dynamics of a spacecraft in orbit about Apophis during the close encounter. The minimum and maximum values of the variations are obtained for the pairs $(\lambda_0, \varepsilon_0) = (19.7^\circ, 60.9^\circ)$ and $(96.4^\circ, 20.6^\circ)$, respectively, as they are shown in Fig. 2. Our results are slightly different from the ones found by Souchay *et al.* (2018), because we use a slightly different and more recent set of physical parameters of the asteroid,

determined by Brozović *et al.* (2018).

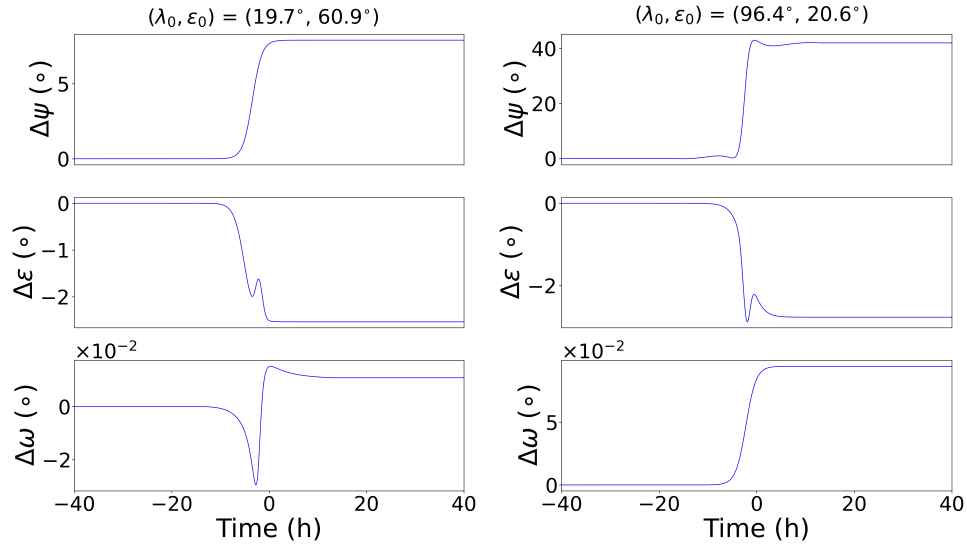


Fig. 2 – Minimum (left column) and Maximum (right column) variations of the orientation of Apophis spin axis.

3. DYNAMICAL MODEL

In the following, we investigate the motion of a spacecraft in orbit around Apophis by taking into account the variations of the spin axis of the target during the close encounter, as calculated and described above. The equations of motion used here are referred to an inertial reference frame with origin at the centre of mass of the asteroid, with two axes along the J2000 ecliptic plane. As done in Aljbaae *et al.* (2020), we consider the asteroid as a cloud of 3996 point masses, corresponding to the number of faces in the Brozović *et al.* (2018) shape model to calculate the gradient of its gravitational potential. For a complete discussion about the validation of this gravitational potential modelling see Aljbaae *et al.* (2020). To reach the accuracy of the orientation and distance from the Earth to Apophis provided by the JPL's HORIZONS ephemerides[‡], we take into account the gravitational influence of the Sun, the eight planets, the Moon, Pluto, and the three largest asteroids, Ceres, Pallas, and Vesta. The initial conditions for all the bodies are provided by JPL's HORIZONS ephemerides on March 1, 2029. We used the Runge-Kutta 7/8 integrator with

[‡]<https://ssd.jpl.nasa.gov/?horizons>

variable step size, optimized for the accuracy of 10^{-12} , to record the orbit every 30 seconds. Our determination for the minimum distance during the encounter is 37723 km, which fits very well with the value of 37728 km given by HORIZONS. The difference between our model and HORIZONS of 5 km is about 0.01% of the minimum distance Earth-Apophis. That makes a difference in the gravitational potential of the earth on the centre of our target of order $4.95 \times 10^{-22} \text{ cm s}^{-2}$. That is really negligible comparing to the surface gravity of the asteroid (0.0023 cm s^{-2}). We tested our Integrator compares the orbits of all the planets in the solar system with Horizon and found very satisfactory results in a short integration period of some months, we just presented the minimum distance as an indicator of the precision. However, integrating for more time will certainly generate bigger errors because we did not consider the same perturbations as the Ephemeris (Such as relativistic perturbations, J_2 of the sun and other plants ... etc.). That is out of the scope of our work and is no needed for such a short time. The gravitational potential of the Earth and of the Moon are expanded using the spherical harmonics up to degree and order 4, as implemented in [Sanchez *et al.* \(2017\)](#) and [Sanchez and Prado \(2014\)](#). Our dynamical model also includes Solar Radiation Pressure (SRP), as described in [Beutler \(2005\)](#), applied only on the spacecraft. We apply this effect for an OSIRIS-REx-like spacecraft with a reflectance of 0.4 and a mass-to-area ratio of 60 kg.m^{-2} . The short period of our integration does not imply any non-gravitational perturbation on the asteroid. Thus the equations of motion for a spacecraft close to (99942) Apophis are given by:

$$\ddot{\mathbf{r}} = U_{\mathbf{r}} + \sum_{i=1}^{14} \mathcal{G}m_i \left(\frac{\mathbf{r}_i - \mathbf{r}}{|\mathbf{r}_i - \mathbf{r}|^3} - \frac{\mathbf{r}_i}{|\mathbf{r}_i|^3} \right) + \mathbf{P}_{\mathbf{E}} + \mathbf{P}_{\mathbf{M}} + \nu \mathbf{P}_{\mathbf{R}} \quad (1)$$

where, \mathbf{r} is the position vector of the spacecraft in the inertial frame of reference, \mathbf{r}_i and $\mathcal{G}m_i$ are the position vector and gravitational parameter of the i^{th} body, with $\mathcal{G} = 6.67259 \times 10^{-20} \text{ km}^3\text{kg}^{-1}\text{s}^{-2}$. $\mathbf{P}_{\mathbf{E}}$ and $\mathbf{P}_{\mathbf{M}}$ are, respectively, the acceleration due to the gravitational potential of the Earth and of the Moon, described by the spherical harmonics up to degree and order 4. $\nu \mathbf{P}_{\mathbf{R}}$ represents the acceleration due to the direct radiation pressure considering the shadowing phenomenon, as described in our previous work ([Aljbaae *et al.*, 2020](#)). $U_{\mathbf{r}}$ is the gradient of the gravitational potential of asteroid, calculated from a sum of 3996 points after rotating the shape [Pravec *et al.* \(2014\)](#) about the origin, in terms of longitude and obliquity. Here, we considered fixed rotation period $P_{\omega} = 27.38 \text{ h}$ and the precession period $P_{\psi} = 263 \text{ h}$ as mentioned in [Brozović *et al.* \(2018\)](#). However, the estimation of these periods during the close approach with our planet is still an open question and should

be considered in future studies. In order to orientate Apophis with respect to our reference frame, we apply a sequence of rotations that can be represented as follows:

$$\begin{aligned} &R_z\left(\frac{2\pi}{p_\psi}t + \lambda_0 + \Delta\psi\right) \\ &R_x(\varepsilon_0 + \Delta\varepsilon) \\ &R_z\left(\frac{2\pi}{p_\omega}t + \Delta\omega\right) \end{aligned} \quad (2)$$

where, R_x and R_z are the rotation matrix about the x-axis and z-axis, respectively. $\Delta\psi$, $\Delta\varepsilon$, and $\Delta\omega$ are the variations of the Apophis axis as calculated in the previous section. Here, we suppose that the shape of the asteroid and the periods p_ω , p_ψ do not change significantly during the Apophis/Earth close encounter. However, this is one of the limitations of our work. The estimation of these changes is still an open question that needs to be investigated.

4. EFFECTS OF THE SPIN AXIS VARIATIONS ON AN ORBIT AROUND APOPHIS

In this section, we investigate the specific effects of the variations of orientation of Apophis spin axis on the orbit of the spacecraft. We consider here the initial values for the minimum and the maximum of these variations, as outlined in section 2. As we are concerned here by the very short time interval of the close encounter, that is to say, a few hours, we do not take into account the gravitational effect of the other bodies of the Solar system and SRP. They are omitted just to isolate the effects of the changes of the Apophis spin axis. Here, we restricted our study to an initial circular retrograde orbit along the equatorial plane of the asteroid ($i = 0^\circ$), by testing successive values of the semi-major axis (a_0) of 0.45, 0.5 and 1.0 km. As already mentioned, we consider the asteroid as a cloud of 3996 point masses (Aljbaae *et al.*, 2020). This approach will generate bigger errors very close to the surface of the asteroid with $a_0 < 0.45$ km. Thus we need a higher-precision model for orbits very close to the surface such as the classical polyhedral approach (Werner, 1997; Tsoulis and Petrović, 2001), which is out of the scope of this work. Our results are presented in Fig. 3. We can notice that the minimum spin variations ($\lambda_0 = 19.7^\circ$, $\varepsilon_0 = 60.9^\circ$) generate bigger effects on the orbits than the maximum spin variations ($\lambda_0 = 96.4^\circ$, $\varepsilon_0 = 20.6^\circ$), as discussed in Sec. 5. Table 1 lists the peak-to-peak amplitude of the variations of the orbital elements in each case, as well as the minimum and maximum period of significant components calculated by the fast Fourier transform (FFT). We remark that these effects are considerably attenuated as the orbit is away from the asteroid, as shown in Fig. 4, where we plot the peak-to-peak amplitudes of the variations of semi-major axis (Δa) and of the eccentricity (Δe) of the spacecraft

Table 1

Effects on a , e and i of the changes of Apophis spin axis during the Earth close encounter, on orbits with $a = 0.45, 0.5, 1.0$ km. All the other orbital parameters are fixed to 0.

| | $\lambda_0 = 19.7^\circ, \varepsilon_0 = 60.9^\circ$ | | | $\lambda_0 = 96.4^\circ, \varepsilon_0 = 20.6^\circ$ | | |
|-------------------------|--|------------------------|-----------------------|--|------------------------|-----------------------|
| | amp. | Min. period. (days) | Max. period (days) | amp. | Min. period. (days) | Max. period (days) |
| | $a_0 = 0.45$ km | | | | | |
| Δa (km) | 0.2155 | 0.3306 | 3.5644 | 0.0570 | 0.1265 | 6.8571 |
| Δe | 0.4045 | 0.1576 | 10.1408 | 0.1394 | 0.1265 | 6.3158 |
| Δi ($^\circ$) | 11.6476 | 0.1680 | 1.3433 | 6.5521 | 0.3784 | 2.6471 |
| | $a_0 = 0.50$ km | | | | | |
| Δa (km) | 0.2047 | 0.1266 | 2.5043 | 0.0474 | 0.1265 | 6.0251 |
| Δe | 0.3004 | 0.1540 | 9.1139 | 0.0953 | 0.1265 | 5.6031 |
| Δi ($^\circ$) | 16.3133 | 0.1308 | 1.9726 | 4.5566 | 0.1265 | 1.4076 |
| | $a_0 = 1.00$ km | | | | | |
| Δa (km) | 0.0221 | 0.1472 | 2.0870 | 0.0075 | 0.1266 | 3.0316 |
| Δe | 0.0374 | 0.1265 | 2.5760 | 0.0125 | 0.1265 | 1.5352 |
| Δi ($^\circ$) | 3.2891 | 0.1290 | 0.1386 | 0.3560 | 0.1265 | 1.5047 |

due to the variations of the spin axis, as a function of the initial value of the semi-major axis. We remark that the values are quite different according to the initial conditions for the Apophis spin axis orientation.

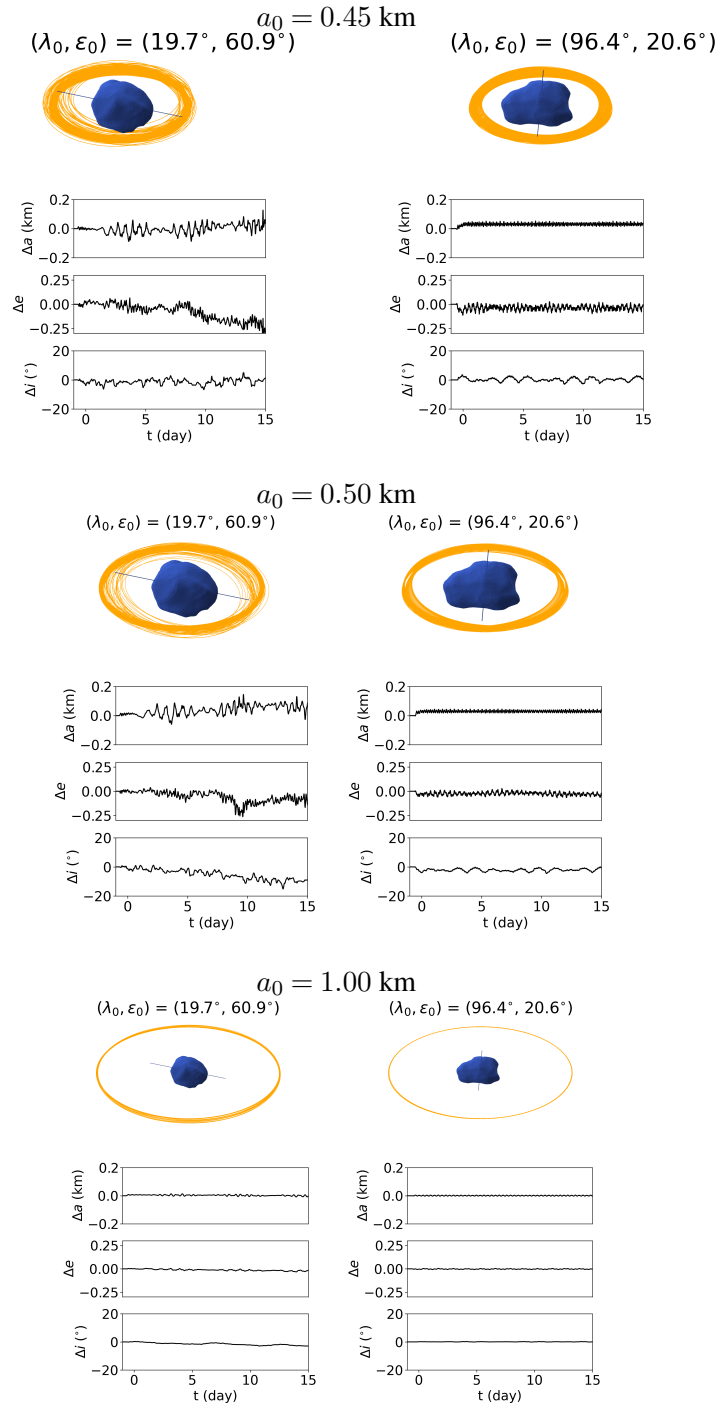


Fig. 3 – Effects on a , e and i of the changes of Apophis spin axis during the Earth close encounter, on orbits with $a = 0.45, 0.5, 1.0 \text{ km}$. All the other orbital parameters are fixed to 0.

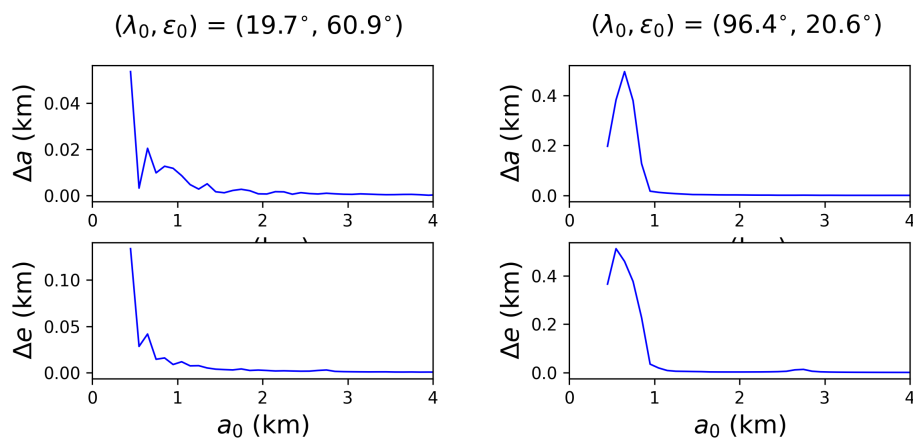


Fig. 4 – Peak-to-peak amplitudes of the variations of semi-major axis (Δa) and eccentricity (Δe) of a spacecraft due to the variations of the spin axis of Apophis, with respect to the initial value of the semi-major axis.

5. STUDY OF THE ORBITAL STABILITY

In this section, we carry out a qualitative analysis of the orbital stability of a spacecraft around Apophis before and after the close encounter with the Earth. We test the two extreme cases of initial conditions of Apophis spin orientation described in Sect. 2, that is to say $(\lambda_0, \varepsilon_0) = (19.7^\circ, 60.9^\circ)$ and $(96.4^\circ, 20.6^\circ)$, referred hereafter as Spin-1 and Spin-2. We consider the full set of perturbations on the spacecraft, mentioned in Sect. 3. We use equation 1 to describe the 60-days motion of the spacecraft around Apophis. The initial conditions of the planets are generated by HORIZONS and set on March 1, 2029. Thus, our 60 days time span covers 43 days before the close encounter and 16 days after. This period was chosen to give the spacecraft enough time to maneuver before the close encounter. In Fig. 5, we show the final states of the orbits integrated for 40-days (top panels) and 60-days (bottom panels). An orbit is considered to characterize an escape from the asteroid when the distance from its centre becomes 3 times larger than the Apophis Hill sphere which is about 34 km. It is considered to characterize a collision with the central body when the particle crosses a 3D ellipsoid of radius $0.235 \times 0.189 \times 0.176$ km. We notice that the large majority of the orbits ($\sim 95\%$) collide or escape from the system just after the close encounter with our planet, whereas the totality of orbits are bounded before. This confirms the conclusion of [Aljbaae et al. \(2020\)](#). We also remark that the initial Apophis spin orientation slightly affects the distribution of the colliding and escaping orbits. This demonstrates that it has to be taken into account for the computations.

In Fig. 6, the level of perturbation after a 40-day integration is characterized by the peak-to-peak amplitude (Δa) of the variations of the semi-major axis. Moreover, we observe that the less perturbed region generated by the case with Spin-1 initial conditions is by far more extended than the one generated by Spin-2. This should come from the irregularity of the projection of the shape of the asteroid on the spacecraft orbital plane. The least perturbed orbit in each case is shown in Fig. 7, which corresponds to $\Delta a = \sim 2$ m for Spin-1 and $\Delta a = \sim 35$ m for Spin-2. It is worth mentioning that the two initial conditions of the spin of the asteroid considered in this work will generate two independent dynamical conditions according to the projection of the shape of the asteroid on the spacecraft orbital plane. Thus, the phenomenon that happens for one condition can be applied of the other.

As noted earlier in this section, the large majority of orbits, integrated for a 60-days time interval, collide or escape because of the close encounter between Apophis and our planet. Indeed, the heavy perturbed system of a particle surrounding Apophis under the influence of the Earth tends to produce by far more chaotic than regular orbits after the encounter. In order to investigate the phase space structure of the orbits, we apply the following three different methods of analysis.

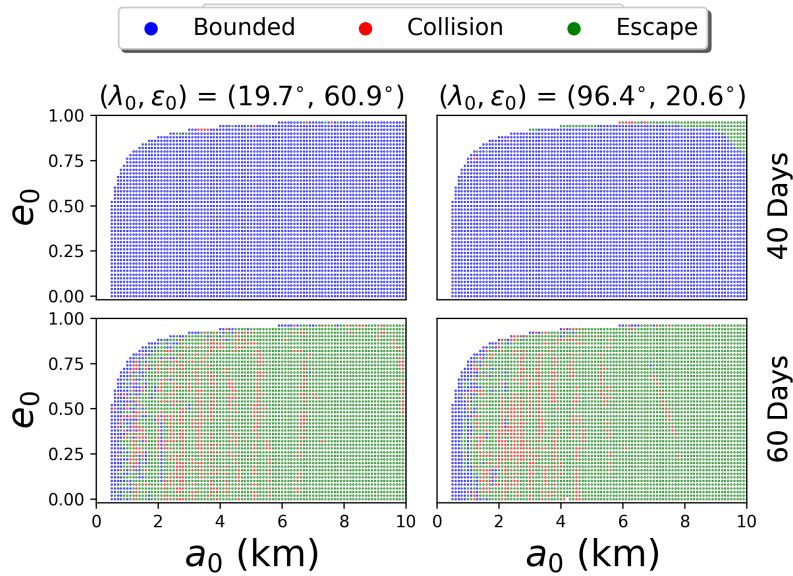


Fig. 5 – Characterization of the orbits around (99942) Apophis for 40 days (Top) and 60 days (Bottom) time span starting from March 1, 2029.

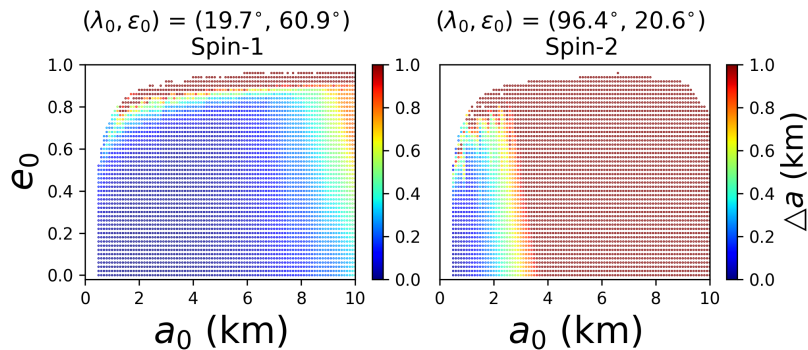


Fig. 6 – Variation maps of the semi-major axis coming from the ensemble perturbations on the real system of Apophis before the close approach with the Earth.

5.1. USE OF THE MEGNO ALGORITHM

In this subsection, we apply the discrete-time version of the Mean Exponential Growth factor of Nearby Orbits developed by [Cincotta and Simó \(2000\)](#). In this method, a global dynamics insight is obtained by calculating the average of the relative divergence of the orbit using the following expression ([Mestre *et al.*, 2011](#))

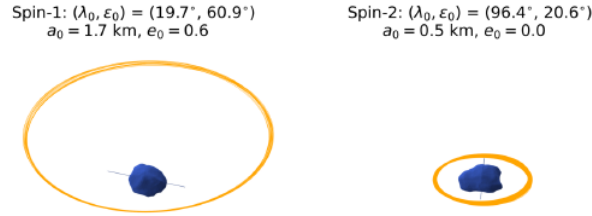


Fig. 7 – Less perturbed orbits around Apophis before the close approach with our planet.

$$\text{MEGNO} = \frac{2}{T} \sum_{k=1}^T k \ln \left(\frac{\delta(k)}{\delta(k-1)} \right) \quad (3)$$

where, $\delta(k)$ represents the deviation vector in the phase space, and T is the total time of integration. Each iteration is building up over 30 seconds from 1 to 60 days. Our results are illustrated in Fig. 8. The larger MEGNO values correspond to a higher degree of chaos and a higher chance of instability. We notice that there are some isolated regions (in dark blue colour) where the spacecraft can maintain quasi-periodic orbits. Some straight lines appear in the map, which could indicate some type of resonance in the system. However, studying these resonances is out of the scope of this work.

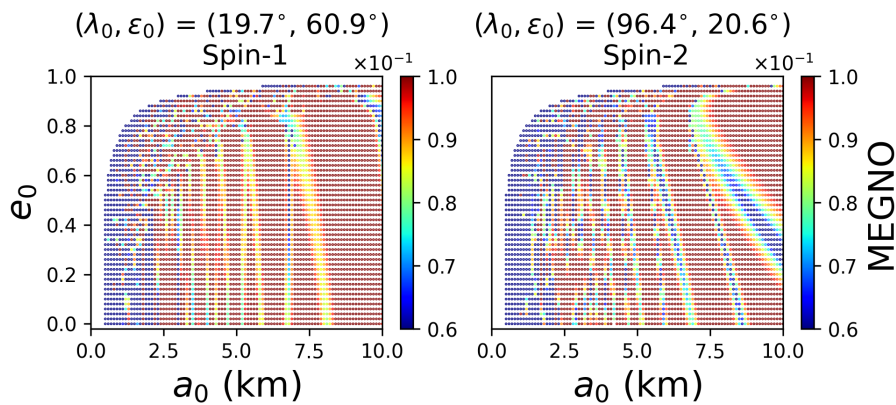


Fig. 8 – MEGNO dynamical maps for the spacecraft orbits around the Apophis system.

5.2. PERTURBATION MAP OF TYPE II (PMAP)

In this method, we calculate the Perturbation Maps of type II, as presented in [Sanchez *et al.* \(2017\)](#); [Sanchez and Prado \(2019\)](#) and [Sanchez *et al.* \(2020\)](#). The perturbations of energy undergone by the spacecraft are measured according to the following expression.

$$PI_{ii} = \frac{1}{T} \int_0^T \langle \mathbf{a}, \frac{\mathbf{v}}{|\mathbf{v}|} \rangle dt, \quad (4)$$

where, \mathbf{a} is the acceleration due to all perturbations to Keplerian motion about Apophis, \mathbf{v} is the velocity of the spacecraft, T is the final time of the numerical integration. In this approach, the value of PI_{ii} gives a good indication of the variation of energy caused by the perturbations. For instance, the blue zone in Fig. 9 corresponds to a negative value of the integral, which indicates a loss of energy and, as a consequence, a decreasing semi-major axis, which could lead to a collision with the asteroid. However, not all collisional orbits have a negative value of this integral. If the orbit collides after about ten days of integration, the integral value is positive, as we will see later. We notice that the zone with negative values of PI_{ii} is compatible with the smallest MEGNO values shown in Fig. 8. In fact, MEGNO is a tool principally devoted to detecting chaos, and after 10 days of integration, the trajectories may not present chaotic behaviour, even if they are highly disturbed as shown by the PMap algorithm. In other words, we can conclude that the PMap method can provide more information close to the central body than the MEGNO method.

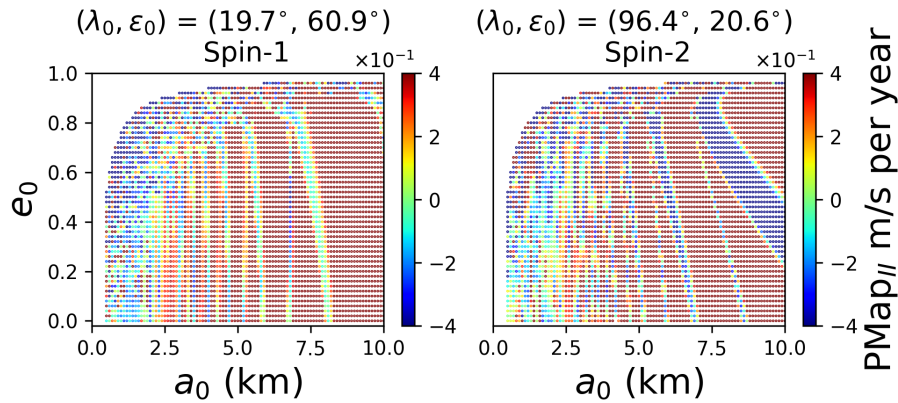


Fig. 9 – Perturbation maps of type II (PMap) for a spacecraft orbiting around Apophis.

5.3. TIME-SERIES PREDICTION

Unlike the previous two methods, time-series prediction does not use the nearby orbits. It relies on computational intelligence in Time-Series forecasting to predict the behaviour of the distribution of orbit coordinates based solely on the past-patterns. We built our model using PYTHON language, KERAS (Beutler, 2005), and TENSORFLOW frameworks (Abadi *et al.*, 2016). The method consists in using a sequence of random variables to create a model fitted to historical data and to apply it to predict the future. The dataset for each orbit consists of 6 features (positions and velocity), recorded every 30 seconds. Each feature has values with varying ranges different from others. Thus, we normalize all the feature values between 0 and 1 before training a neural network. The first 90% of the points in each orbit (54 days) are used to train the model and predict the position of the spacecraft during the last 6 days of the orbit. The Earth encounter happened after 43 days of the integration, Thus our training included 11 days after the encounter. In this way, we guaranty that perturbation of the close is among our training data. In each orbit, we have 172800 points, 155520 of them in our training data. That is more than enough to predict the rest of the 18280 points in each orbit. To optimize the performance, our model collects data for the first 12 hours (1440 observations), which are sampled every 2.5 minutes. The positions after 15 observations are used as a label. Our training is interrupted when the validation loss is no longer improving. More details about the method are presented in the Keras documentation pages available at <https://keras.io/>. Then, we calculate the area between the predicted and real data (\mathcal{A}). The smaller the area, the more predictable the orbit, which makes the spacecraft mission much easier to be mapped and planned out. In Fig. 10 we present an example of a bounded orbit and an orbit undergoing an escape after about 45 days, considering both the Spin-1 and Spin-2 conditions.

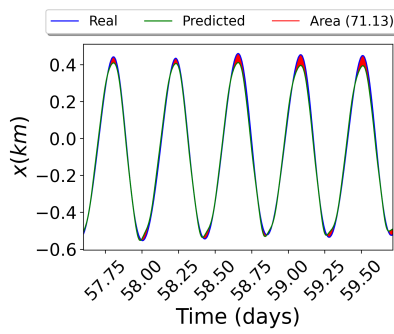
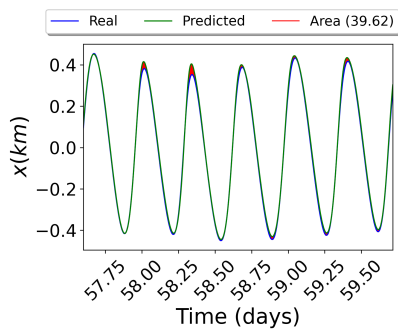
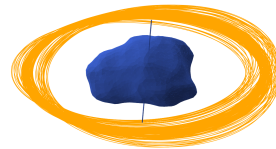
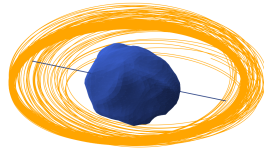
The Forecasting map using the area \mathcal{A} normalized between 0 and 1 is presented in Fig. 11. From Figs. 8, 9, and 11 we notice that the three methods investigated here are conceptually compatible. Although the results are quite similar after $a_0 = 5.0$ km, it seems that PMap shows more details for the orbits closer to the asteroid. For instance, taking the two neighbouring orbits ($a_0 = 0.5$, $e_0 = 0.12$) and ($a_0 = 0.6$, $e_0 = 0.12$), we notice that the first orbit collides with the asteroid after 21 days, while the second one survives the 60-days integration (Fig. 12). These orbits are stated in the PMap in a different category taking the values of 0.8 m/s and -0.45 m/s per year, respectively. However, they are represented by close values in the MEGNO and Time-Series prediction maps.

5.4. COMPARISON OF THE THREE METHODS

Finally, we evaluate the coherence between the three methods presented above, using the Pearson correlation coefficient (Pearson , 1895), which measures a linear relationship between two given variables, denoted by the standard formula presented in Carruba *et al.* (2021), where the authors identified the similarity between four chaos indicators: the Fast Lyapunov exponents (Froeschlé and Lega , 2000), MEGNO, the frequency analysis method (Laskar , 1990), and the auto-correlation function (Carruba *et al.*, 2021). The Pearson correlation coefficient always ranges from -1.0 (anti-correlation) +1.0 (correlation). As the value is close to 0 there is an independence of the variables. Our results are presented in Fig. 13. We found that the PMap and the Time-Series methods are highly correlated.

Spin-1: $(\lambda_0, \epsilon_0) = (19.7^\circ, 60.9^\circ)$
 $a_0 = 0.5 \text{ km}, e_0 = 0.0$

Spin-2: $(\lambda_0, \epsilon_0) = (96.4^\circ, 20.6^\circ)$
 $a_0 = 0.5 \text{ km}, e_0 = 0.0$



Spin-1: $(\lambda_0, \epsilon_0) = (19.7^\circ, 60.9^\circ)$
 $a_0 = 4.6 \text{ km}, e_0 = 0.0$

Spin-2: $(\lambda_0, \epsilon_0) = (96.4^\circ, 20.6^\circ)$
 $a_0 = 4.6 \text{ km}, e_0 = 0.0$

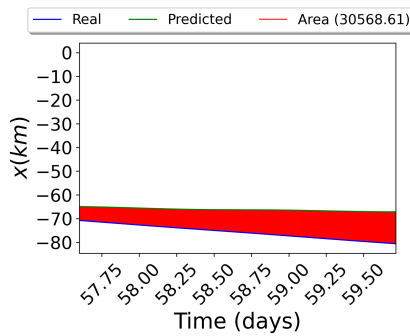
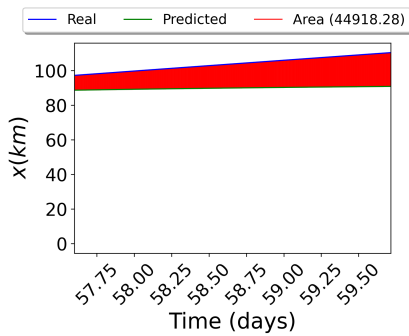
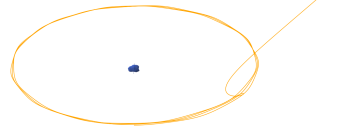
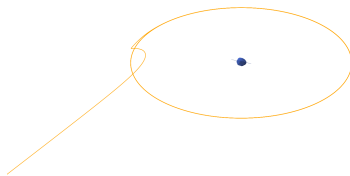


Fig. 10 – Example of a regular (Top panel) and an irregular orbit (Bottom panel) for a spacecraft orbiting around Apophis with the area between the predicted and real data.

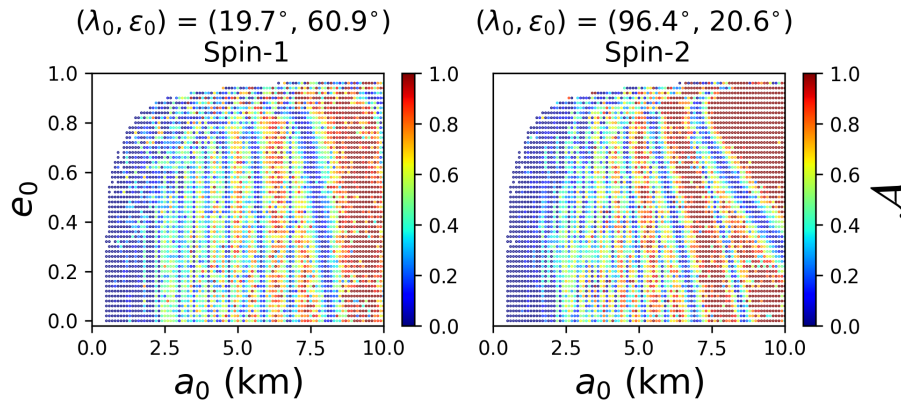


Fig. 11 – Forecasting maps using the Time-Series prediction for orbits around Apophis.

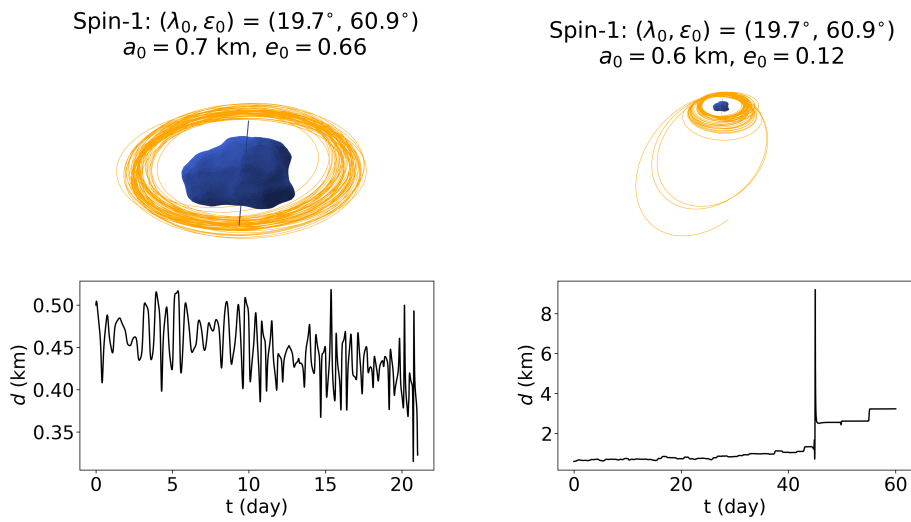


Fig. 12 – Example of two neighbour orbits in the system of Apophis.

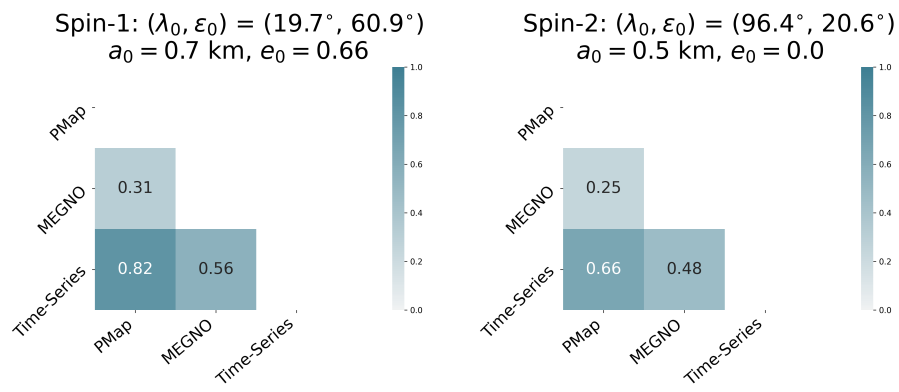


Fig. 13 – Correlation matrix for the three methods used to investigate the phase space structure associated to Apophis.

6. CONCLUSIONS

In this work, we investigated the dynamics of a spacecraft orbiting around asteroid (99942) Apophis during its 2029 close encounter with the Earth, considering the dependence on the initial conditions of the rotation of the target. We used the dynamical model developed in our previous work (Aljbaae *et al.*, 2020), for which we represented the gravitational field of the asteroid by a cloud of 3996 point masses system distributed inside a polyhedral shape derived from Brozović *et al.* (2018). We applied the method of Souchay *et al.* (2018) to determine the changes of Apophis' spin state due to the terrestrial torques during the close encounter. In a first step, we explored the impact of this phenomenon on the dynamics of a spacecraft orbiting around the asteroid, considering two cases of initial spin orientation, corresponding respectively to the minimum and maximum values of the spin variations during the encounter.

We showed that this orientation can influence significantly the behaviour of the orbital motion of the spacecraft. In a second step we carried out a 60-days integration ranging 43 days before and 16 days after the encounter and studied the dependence of the stability of orbits with respect to the initial value of the semi-major axis. We found that the very large majority of cases, the spacecraft undergoes a collision or escapes due to the perturbation caused by the close encounter, whereas it shows in all cases a very stable orbit before. Then we applied three different methods *i.e.* MEGNO, PMap and Time Series Forecasting to characterize in a deeper way the degree of stability or chaoticity of the orbits. The Time-Series Forecasting is used to classify orbits based on a relationship between the difficulty in the prediction and the stability. Using this method, we isolated the most predictable orbits that could be a stable ones in the system. A good correlation was found between this approach and MEGNO (Cincotta and Simó, 2000) or the *Perturbation Map* (PMap) of type *II* (Sanchez *et al.*, 2017; Sanchez and Prado, 2019). However, we showed that PMap provides more information for orbits close to the central body. That could come from the short integration time of 60 days considered in this work. The objective of this paper is no more an attempt to help to the preparation of a hypothetical future plan for a mission around Apophis, than to carry out a realistic analysis of the interesting problem of celestial mechanics dealing with the dynamical behaviour of a spacecraft around an asteroid undergoing the gravitational effects caused by a close encounter with the Earth.

Acknowledgements. The authors would like to thank the Coordination for the Improvement of Higher Education Personnel (CAPES) which supported this work via the grant 88887.374148/2019-

00. VC acknowledge the support of the Brazilian National Research Council (CNPq, grant 301577/2017-0).

APPENDIX 1: THE VARIATIONS OF APOPHIS AXIS

In this appendix, we present the variations of the precession in longitude ($\Delta\psi$), obliquity ($\Delta\varepsilon$), and rotation angle ($\Delta\omega$) of the asteroid, as presented in [Souchay *et al.* \(2018\)](#)

$$\begin{aligned}\Delta\psi &= \frac{3GM_{\oplus}}{2a^3\omega} H_d \int \cos I \left(\frac{a}{r}\right)^3 \left(1 - \cos 2(\lambda - h)\right) dt - \\ &\quad \frac{3GM_{\oplus}}{2a^3\omega} H_t \int \left[\left(\frac{a}{r}\right)^3 (2 \cos I \cos 2(l + g)) - \right. \\ &\quad \quad (1 + \cos I) \cos 2(\lambda - h - l - g) + \\ &\quad \quad \left. (1 - \cos I) \cos 2(\lambda - h + l + g) \right] dt \\ \Delta\varepsilon &= \frac{3GM_{\oplus}}{2a^3\omega} H_d \int \sin I \left(\frac{a}{r}\right)^3 \sin 2(\lambda - h) dt + \\ &\quad K' \int \cos I \left(\frac{a}{r}\right)^3 \sin I \sin 2(l + g) dt + \\ &\quad \frac{3GM_{\oplus}}{2a^3\omega} H_t \int \frac{1}{\sin I} \left(\frac{a}{r}\right)^3 \left[(1 + \cos I)^2 \sin 2(\lambda - h - l - g) + \right. \\ &\quad \quad \left. (1 - \cos I)^2 \sin 2(\lambda - h + l + g) \right] dt - \\ &\quad \frac{3GM_{\oplus}}{2a^3\omega} H_t \int \frac{\cos I}{\sin I} \left(\frac{a}{r}\right)^3 \left[(1 + \cos I)^2 \sin 2(\lambda - h - l - g) - \right. \\ &\quad \quad \left. (1 - \cos I)^2 \sin 2(\lambda - h + l + g) \right] dt \\ \Delta\omega &= \frac{2\pi k_2}{0.334 * T_0} \int \frac{M_{\oplus}}{M_a} \left(\frac{a}{r}\right)^3 \left(\sin^2 \delta - \frac{1}{3} \right)\end{aligned}$$

where $M_{\oplus} = 5.972 \times 10^{24}$, $M_a = 5.310 \times 10^{10}$ kg are, respectively, the mass of the Earth and the mass of Apophis, k_2 is the Love number of the asteroid. An arbitrary value of 0.25 was chosen following the theoretical discussions of the static and dynamic Love numbers of asteroids ([Jacobson and Scheeres, 2011](#); [Efroimsky, 2015](#)).

$T_0 = 30.4$ h is the nominal value of the rotation period, estimated from the rotation light-curves (Pravec *et al.*, 2014). $a = 37725$ km is the minimum distance between the geocenter and Apophis during the 2029 encounter. r is the distance Apophis-Earth. l, g and h are the Andoyer rotational angles. I and λ are, respectively, the obliquity and longitude angle of the Earth centre with respect to the direction of the Earth at its minimum distance (see Fig. 1). δ is the declination of the Earth with respect to Apophis equatorial plane ($\sin \delta = \sin I \sin \lambda$). ω is the spin rate of the asteroid. $H_d = \frac{2C-A-B}{2C}$ and $H_t = \frac{B-A}{4C}$ are constants related to the dynamical flattening and tri-axiality of Apophis. A, B and C are the moments of inertia along the principal axis of the asteroid (Aljbaae *et al.*, 2020). More details on these equations can be found in Souchay *et al.* (2018, 2014a,b)

REFERENCES

- Abadi, M. and 21 colleagues: 2016. *arXiv* **1605.08695**.
- Aljbaae, S. and 6 colleagues: 2020. *Romanian Astron. J.* **31**, 3, 241-263
- Beutler, G.: 2005. Springer, ISBN 3-540-40750-2.
- Brozović, M. and 17 colleagues: 2018. *Icarus* **300**, 115-128.
- Carruba, V., Aljbaae, S., Domingos, R. C., Huaman, M., Barletta, W.: 2021. *Celestial Mech.* **133**.
- Chollet François.: 2017. Manning, ISBN 9781638352044. <https://keras.io>.
- Cincotta, P. M., Simó, C.: 2000. *A&A Supplement Series* **147**, 205-228.
- Efroimsky, M.: 2015. *The Astronomical Journal* **150**.
- Froeschlé, C., Lega, E.: 2000. *Celestial Mech.* **78**, 167-195.
- Jacobson, S. A., Scheeres, D. J.: 2011. *The Astrophysical Journal* **736**.
- Kinoshita, H.: 1978. *Celestial Mech.* **15**, 277-326
- Laskar, J.: 1990. *Icarus* **88**, 266-291.
- Mestre, M. F., Cincotta, P. M., Giordano, C. M.: 2011. *MNRAS* **414**, L100-L103.
- Müller, T. G. and 6 colleagues: 2014. *A&A* **566**.
- Pearson, K.: 1895. *Proceedings of the Royal Society of London Series I* **58**, 240-242.
- Pravec, P. and 19 colleagues: 2014. *Icarus* **233**, 48-60.
- Sanchez, M. D. and Prado F. B. A.: 2017. *AAS/AIAA Astrodynamics Specialist Conference* **162**.
- Sanchez, D. M., Prado, A. F. B. A., Yokoyama, T.: 2014. *ASR* **54**, 1008-1018.
- Sanchez, D. M., Deienno, R., Prado, A. F. B. A., Howell, K. C.: 2020. *MNRAS* **496**, 2085-2097.
- Sanchez, D. M., Prado, A. F. B. A.: 2019. *Journal of Spacecraft and Rockets* **56**, 1775-1785.
- Scheeres, D. and 5 colleagues: 2005. *Icarus* **178**, 281-283.
- Souchay, J., Lhotka, C., Heron, G., Hervé, Y., Puente, V., Folgueira Lopez, M.: 2018. *A&A* **617**.
- Souchay, J., Souami, D., Lhotka, C., Puente, V., Folgueira, M.: 2014. *A&A* **563**.
- Souchay, J., Heron, G., Puente, V., Lopes, M. F.: 2014. *Romanian Astron. J.* **24**, 87.
- Tsoullis, D., Petrović, S.: 2001. *Geophysics* **66**, 535.
- Werner, R. A.: 1997. *Computers and Geosciences* **23**, 1071-1077.

Received on 2 August 2021